Broadband Characterization of Silicate Materials for Potential 5G/6G Applications

Rocio Rodriguez-Cano, Steven Perini, Brian Foley and Michael Lanagan

***Abstract*—This paper provides a broadband dielectric characterization of different silicate substrates up to 115 GHz, to fill the gap of the properties of different kinds of glasses in a broad part of the mm-wave spectrum. Both the internal structure (crystalline or amorphous) and the chemistry of the substrates has an influence in the permittivity and loss tangent of the material. Quartz and sapphire are crystalline materials that exhibit low loss in the mm-wave frequency range. Amorphous silicates generally have higher loss values than crystalline materials, and within the glasses, the level of impurities added also affects the dielectric loss. Several characterization techniques have been employed to cover a broad frequency band. The limitations of the different characterization techniques are also included. Once the dielectric properties of substrates are characterized, a metasurface has been designed and fabricated at 100 GHz to increase the reflection in window glass and provide coverage on areas that would otherwise be shadowed. The measurement results are in good agreement with the simulations.**

***Index Terms*—Characterization, dielectric loss, material, metasurface, glass, transparent, 5G, 6G.**

I. Introduction

THE inclusion of new frequency bands in the millimeter-wave (mm-wave) spectrum for the fifth generation of mobile communications (5G) entails new challenges from the signal propagation perspective. The new mm-wave frequency bands proposed in the 5G standardization are FR2-1: 24.25-52.6 GHz and FR2-2: 52.6- 71 GHz [1]. Frequencies above 100 GHz are being studied for 6G [2]. Higher frequencies can be translated into shorter wavelengths, which are more sensitive to the propagation environment [3]. The propagation losses caused by the materials that constitute the buildings, such as glass, are more important for the link budget in the mm-wave spectrum than in the sub-7 GHz bands. Besides, the low available space left in mobile phones has forced the manufacturers to place the new mm-wave antenna modules on the edges of the phone and below the glass back cover [4]. Glass is receiving a lot of attention for the next generation of mobile communications (6G) as well, as the concepts of reconfigurable intelligent surface (RIS) or large intelligent surface (LIS) begin to appear in the literature [5]–[7]. RIS consists of an array of reflecting elements that allow the reconfiguration of the incoming signal by controlling the phase shift of each reflecting element. Its function is to increase the channel gain and to offer coverage to shadowed areas that are covered by major obstacles. These surfaces can be placed on the building windows, facades, billboards, cars, etc., to increase the coverage radius of mm-wave base stations. The concept can also be applied inside buildings. In the study carried out in an indoors environment in [8] from 110 GHz to 170 GHz, most of the energy at the receptor was provided by large reflecting surfaces.

Few point measurements of glass attenuation have been reported in the mm-wave frequency bands. In [9], the attenuation of clear glass is provided at only three frequency points: 28, 73 and 91 GHz. The clear glass has the highest attenuation among all the measured materials: plywood, drywall, cinder block and acoustic ceiling tiles. For clear glass, the mean attenuation is 4.38, 14.37 and 18.78 dB/cm, respectively for 28, 73 and 91 GHz. In [10], the measured total attenuation at 38 GHz for a modern 2-layered energy efficient glass window is 25 dB.

However, there is only limited dielectric loss and permittivity data for glass in the literature for the mm-wave frequency bands [11]–[14]. The most extensive, [14], shows the difference between alkali and alkali-free aluminoborosilicate glass, but it does not differentiate the most common glasses available. Moreover, the glass manufacturers only provide the dielectric properties below 3 GHz. From the structure simulation perspective, the electromagnetic software uses the superposition of first and second order Debye model to obtain the dielectric constant in broadband simulations with dispersive materials, but there is no evidence of its accuracy when there are no measurement data results to compare it with. Besides, the software has a limited material library that does not include many different silicates. Antenna and metasurface designers for the next generations require the characterization of the dielectric properties of the different glasses, for accurate simulations in the mm-wave spectrum. Most of the publications only use one measurement technique to obtain the data. In this paper, we have combined four different measurement techniques to obtain the response in a broad bandwidth. We have also focused on the silicate family, as there are four orders of magnitude of difference in the loss. As the dielectric loss is higher in the mm-wave spectrum than the metal loss, cheap silicate substrates with low loss are essential for the devices of the next generations of communications. Therefore, it is important to characterize both glass and the rest of the silicate family. We have also included a study of the contribution to loss of different silicates and different metals in a common metasurface at 100 GHz.

This paper is organized as follows: Section II describes the

This work was supported in part by the National Science Foundation as part of the Center for Dielectrics and Piezoelectrics under Grant Nos. IIP-1841453 and IIP-1841466, and by a research grant (41389) from VILLUM FONDEN.

Rocio Rodriguez-Cano, Steven Perini, Brian Foley and Michael Lanagan are with the Materials Research Institute, Penn State University, University Park, PA 16802 USA. Rocio Rodriguez-Cano is also with the APMS section, Department of Electronic Systems, Aalborg University, 9220 Aalborg East, Denmark.

difference among the materials in the silicate family, in terms of internal structure and composition, which will be relevant to understand the difference in dielectric properties. Section III covers the different dielectric relaxation mechanisms along the frequency spectrum. These mechanisms affect the permittivity and loss tangent of the materials. Just to clarify, the terms permittivity, dielectric constant and ϵ_r (with the subscript r meaning relative) are used throughout the paper to refer to the real part of the complex permittivity. Section IV provides the dielectric measurement results obtained with different measurement techniques to cover a broad frequency band. Finally, in Section V, a proof-of-concept reflecting metasurface has been designed and manufactured with the dielectric parameters obtained at 100 GHz, to test the accuracy of the dielectric properties measurement of window glass.

II. Silicate Materials

As was mentioned in the introduction, transparent materials, such as glass, play an important role in 5G communications and beyond. For that reason, it is crucial to assess the frequency dependent dielectric properties of the different silicate materials. There are two ways in which they can be assorted. On one hand, they can be classified according to their internal structure (see Fig. 1). Sapphire and quartz have a crystalline structure, while fused silica (FS) and modified glasses have amorphous structures. The expanded amorphous structure affords more molecular movement and additional electric polarizability, resulting in higher dielectric loss [15]. On the other hand, the composition of the materials also affects the loss tangent. Silicates are mainly composed of silicon dioxide (SiO_2). Alkali and alkaline earth modifiers are added to fused silica to reduce the melting temperature [16]. Additives such as aluminum and boron are added as part of the silica network [17]. The composition of some of the assessed materials has been obtained through an inductively coupled (ICP) analysis and is listed in Table I. As it can be seen, the fused silicas present the highest percentage of (SiO_2), while AF45 glass has the lowest concentration. Sapphire is made of aluminium oxide (Al_2O_3) and has been included in the study as a reference of crystalline material.

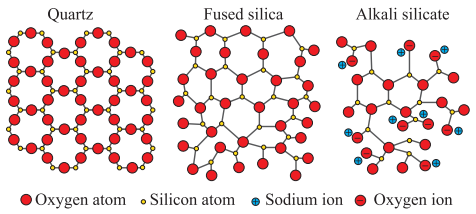

Fig. 1. Internal structure of the different silicate materials.

III. Dielectric loss mechanisms

The role of crystal structure on intrinsic and extrinsic dielectric loss in the microwave frequency range has been extensively studied. Microwave loss contributions from infrared active lattice modes have been correlated with oscillator strength and frequency in high-Q ceramics [18]. Additional losses have been associated with point defects such as oxygen vacancies and site disorder [19]. Significantly fewer studies have been devoted to the effects of glass structure and chemistry on microwave and mm-wave dielectric loss.

Electronic conductivity has significantly increased loss tangent in titania ceramics where 3 GHz loss values of 6×10^{-5} have increased to 4×10^{-4} with small amounts of sodium addition [20]. Alkali additions to glass increase the DC conduction and could also contribute to loss in the microwave and mm-wave frequency range.

The internal structure and composition of materials have a strong influence on dielectric polarization mechanisms. Dielectric materials are composed of electric charge carriers that are polarized to compensate for an external electric field applied, such that opposite charges move in opposite directions. The electric field can cause an electric moment in either atom, ion or molecule [21], [22]. The frequency dependence of the polarization mechanisms and their effect in the real and imaginary parts of the dielectric constant are represented in Fig. 2.

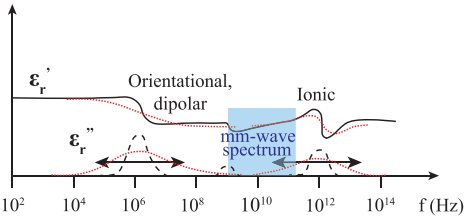

Fig. 2. Effect of the polarization mechanisms affecting the real and imaginary parts of the dielectric constant as a function of the frequencies of interest. The tails of the polarization mechanisms have been represented in red. Re-plotted from [22].

At frequencies below 10^{10} Hz, the dipolar polarization is the predominant mechanism. Molecules that have asymmetric charge distributions change their orientation with an external electric field. Some materials present several dipolar relaxations at different frequencies depending on their composition. Many polymers have a main chain dipole relaxation at $10^4 - 10^6$ Hz. For most polymers, the small relaxation that occurs at 10^9 Hz is due to side group dipoles [23]–[25]. The dielectric relaxations plotted in Fig. 2 are shown at generic frequencies. Specific relaxation frequencies be higher or lower and the breadth of the response is controlled by the distribution of dipole environments within the material. Ionic polarization occurs below 10^{13} Hz, in structures in which atoms are not shared equally, and the electron clouds are displaced towards the stronger binding atoms or when the charged atoms are displaced with respect to each other [26].

For the frequency bands of interest in this paper, low frequency tails of the ionic relaxations might have an impact in the properties of the materials, and it is possible that local conduction of ions also contribute to loss.

TABLE I
INDUCTIVELY COUPLED PLASMA (ICP) ANALYSIS MEASUREMENT RESULTS FOR SOME OF THE SAMPLES.

Material/Composites	SiO_2 (%)	B_2O_3 (%)	Al_2O_3 (%)	K_2O (%)	Na_2O (%)	Li_2O (%)	BaO (%)	CaO (%)	MgO (%)	SrO (%)
Gorilla Glass	61.7	3.72	19.4	1.48	11.6	0.01	0.00	0.00	1.43	0.00
Borofloat 33	80.7	12.0	2.33	0.63	3.58	0.01	0.01	0.00	0.03	0.01
BK7	70.4	10.5	0.22	10.3	7.72	0.01	1.09	0.00	0.03	0.00
AF45	51.1		11.7		0.13		23.4	0.00		
FS 518	101	0.09	0.00	0.00	0.01	0.01	0.01	0.00	0.02	0.00
FS JGS2	97.9		0.01		0.02		0.00	0.00		

TABLE II
DIELECTRIC MEASUREMENT TECHNIQUES.

Technique	Frequency range	Loss threshold	Sample dimensions	Max. thickness	Accuracy
Split-post	Single freq. below 5.17 GHz	10^{-5}	Min. size 3 cm $\times$3 cm. Max. width 9 cm	1.95 mm	$\Delta\epsilon_r/\epsilon_r = \pm(0.0015 + \Delta t/t)$ $\Delta \tan\delta = \pm 2e^{-5}$
Split cavity	Single freq. below 20 GHz	10^{-4}	Min. diameter 2.5 cm	3 mm	$\epsilon_r \pm 1$ %, $\Delta \tan\delta < 1e^{-4}$
Open resonator	15- 67 GHz	10^{-5}	10 cm $\times$10 cm	$< \lambda/4$	$\epsilon_r \pm 0.25$ % [30]
MCK from SWISSto12	70-115 GHz	10^{-3}	Min. size 4 cm $\times$4 cm	20 mm	$\epsilon_r \pm 1$ %, $\tan\delta \pm 5$ %

IV. BROADBAND DIELECTRIC CHARACTERIZATION

Material characterization in a broad frequency band is challenging task, as each different technique only provides a limited bandwidth or a single frequency measurement. Moreover, the thickness requirement and lateral dimensions of the samples vary from one method to another. There is also a limitation in the measurable dielectric loss intrinsic to each technique. This loss tangent measurement floor restricts the measurable frequency range of low loss samples, such as quartz and sapphire, for some techniques.

1) Characterization techniques employed: The characterization techniques used in this paper can be divided into resonance and transmission, and the resonance techniques are further divided into two groups: dielectric resonance techniques and cavity perturbation techniques. In the former, the sample itself acts as a dielectric resonator, and in the latter, the resonance is supported by the metallic walls of the cavity and the sample presence modifies the field distributions in the cavity [27]. In the case of the resonant techniques, the experimental method consists of measuring the Q factor of the empty device and compare it with the quality factor loaded with the sample. The Q factor is defined as the resonance frequency divided by the 3-dB bandwidth. The loss tangent is inversely proportional to the Q factor. On the other hand, the permittivity of the dielectric is related to the perturbation of the resonant frequency [28]. For transmission techniques, the dielectric parameters are extracted from the measured S parameters, using the precision model described in [29]. The different techniques employed are shown in Fig. 3 and are described below.

The parallel plate capacitor technique consists of placing a dielectric sheet between conducting plates, and measuring the capacitance and loss tangent. The precision LCR meter E4980A has been employed in the measurements. From the capacitance, it is possible to obtain the dielectric constant, as follows:

$$C = \frac{\epsilon_r \epsilon_0 A}{d}, \tag{1}$$

where C is the capacitance, ϵ_r is the dielectric constant, ϵ_0 is the permittivity of free space, A is the area of the plates, and d is the plate separation [31]. This technique requires a proper determination of the area when the sample has an arbitrary shape, to avoid introducing errors in the measurement. It has an accuracy of ± 0.05 % for the capacitance, and ± 0.0005 % for the dissipation factor.

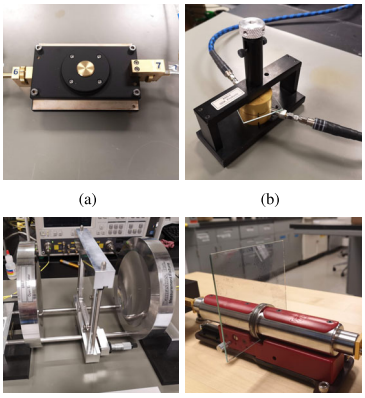

(a) (b) (c) (d)

Fig. 3. Characterization techniques employed. (a) Split-post dielectric resonator (b) Split cavity. (c) Open resonator. (d) MCK from SWISSto12.

The split-post dielectric resonator (SPDR) from QWED is the measurement method that can provide one of the most accurate loss tangent values for low loss dielectric materials. It employs the $TE_{01\delta}$ mode, so that the electric field component is in the azimuth direction. This makes the system insensitive to the presence of air gaps in the z-axis of the fixture [32]. One disadvantage is that only a single frequency point can be measured for each sample, depending on the size of the resonator. The nominal frequency of the employed one is 5.1 GHz. It has also a maximum dimensions and thickness requirement, that can be found in Table II, as well as the method accuracy. To avoid introducing errors in the measurement, the minimum value of the S_{11} and S_{22} should coincide. The split-post has nuts on the side walls of the resonator to adjust the coupling

loops.

The split-cylinder resonator technique, split cavity or resonant mode dielectrometer (RMD-C, GDK Product Inc.) uses a cylindrical cavity separated in two halves. A TE_{011} resonance is excited and from the perturbation of the quality factor, the dielectric properties can be obtained [33]–[35]. The frequency of operation is determined by the diameter and length of the cavity. The alignment of the two circular waveguides is important to avoid any air gaps. The specimen under test should be flat, uniformly thick, and large enough to cover a circle at least 20 % greater in diameter than the cavity. The extension of the sample into the gap is equivalent to replacing a short section of cavity wall by an inductance. To correct for the gap, a factor is used, obtained by a perturbation calculation [36]. The uncertainty from this approximation in the dielectric constant is less than 1 % if the ratio of the sample thickness to waveguide diameter is less than 0.18. This technique can measure thicker and larger samples than the split-post. However, the loss tangent threshold is worse.

The Fabry-Perot open resonator from Damaskos, Inc. allows the sample characterization from microwaves up to low mm-wave bands. The modes to select are the TEM_{00q} modes, where q is the longitudinal mode order. The electric field has a smooth spatial distribution at a transverse cross section that can be compared to a Gaussian function [37], [38]. Therefore, placing the sample at the exact center is critical for this measurement. The open resonator includes a software package to guide through the calibration, measurement and data processing steps. A limited number of resonances can be measured at a given spacing (around 10). With an estimated permittivity and sample thickness, the software calculates the frequencies of the resonant modes. During the measurement, the program searches for the peaks at those frequencies. The open resonator has many modes and some of these may interfere with the modes of interest. It is possible that the peak of interest is shifted and that the program takes another resonance instead. A parameter to indicate the quality of the fitting is included to discard resonances that should be rejected due to interferences. For this reason, this technique has a long calibration and measurement time. Model 600T of the open resonator can be set to any spacing from 11 cm to 29 cm. However, it is unstable at 15.24 cm and 30.48 cm. The manufacturer recommends the spacing 21.3 cm for good overall performance. It is important to consider that different spacings will provide different maximum measurable Q factors. Larger spacings are better for high frequency measurements. This method also requires very large samples (10 cm $\times$ 10 cm).

The material characterization kit (MCK) from SWISSto12, behaves similarly to the free-space techniques with the difference that the waves travel enclosed in corrugated circular waveguides. The excited mode is the HE_{11}, in which the electric field component is pointing upwards. The transitions to convert from the TE_{10} in the rectangular waveguides to the HE_{11} mode, at the input of the corrugated antennas, are included in the MCK. At the end of the antennas, the Gaussian beam launched, provides a plane-wave illumination of the sample [39]. The minimum sample thickness follows the same characterization guidelines than free-space measurements, in which the samples should be thick enough to contain $20°$ of phase at the wavelength of interest. In our model, at 70 GHz, $\frac{20}{360} \times \lambda = 0.23$ mm [39]. Time-domain gating is applied to remove the spurious reflections and then the signal is transformed to the frequency domain. To avoid errors in the extracted material parameters, the gate width should be larger than the width of the desired signal. The S-parameters are employed to obtain the material properties [29], [40]. It gives good permittivity estimates up to 115 GHz, but uncertain estimates for the loss tangent of materials with lower loss than 10^{-3}. In those cases, the measured value should just be taken as an upper limit. A more detailed study about the uncertainties with this technique is found in [39].

The measuring devices need to be connected to a VNA. The S_{21} magnitude uncertainty is below 0.15 dB, and below 0.02 dB for the S_{11}.

2) Dielectric loss and permittivity measurement results: Fig. 4 shows the dielectric constant and loss tangent of the different silicate materials assessed until 115 GHz. The thickness of the materials can be found in Table III. The room temperature during the measurements was $21°$C. The dielectric constant of glasses is limited between 5.5 and 7, though Borofloat 33 has a value of 4.4. The boron ion has a very low polarizability and thus has a very small contribution to the dielectric permittivity. Quartz and sapphire have permittivity values of 4.4 and 9.1, respectively which align with theoretical calculations from polarizability and molar volume [41]. The permittivity values of the different fused silicas are lower than the one of quartz, as their density is lower [15].

TABLE III
THICKNESS OF THE CHARACTERIZED MATERIALS.

Material	Thickness (mm)	Material	Thickness (mm)
Sapphire	0.65	BK7	0.5
Quartz	0.5	Borofloat 33	0.5
FS-518	0.5	Gorilla Glass	0.5
FS-JGS2	1	AF45	0.31
FS-HFM002.B2	0.515	OA-10G	0.7
FS-7980	0.5	Window glass	2.3

For resonant measurement techniques, the minimum measurable loss depends on the Q factor of the resonator, as the power losses limiting the Q factor are added in parallel. If the loaded quality factor is larger than the empty Q factor, the Q factor of the dielectric sample will be dominated by the quality factor of the empty resonator. The loss tangent is inversely proportional to the quality factor of the sample. When the sample Q factor is limited by the Q factor of the empty resonator, it means that the loss tangent value has reached the measurement floor of that particular technique. Those values have been circled in Fig. 4(b). The materials with a crystalline structure, i.e. quartz and sapphire, present the lowest loss tangent values due to the intrinsic nature of the single crystals. Among the materials with an amorphous internal structure, fused silica has a lower dielectric loss, about an order of magnitude above the materials with crystalline structure. From the inductively coupled plasma (ICP) analysis performed in some of the samples, the purity of fused silica was above 97% for JGS2 and the one labeled as FS 518 does not have

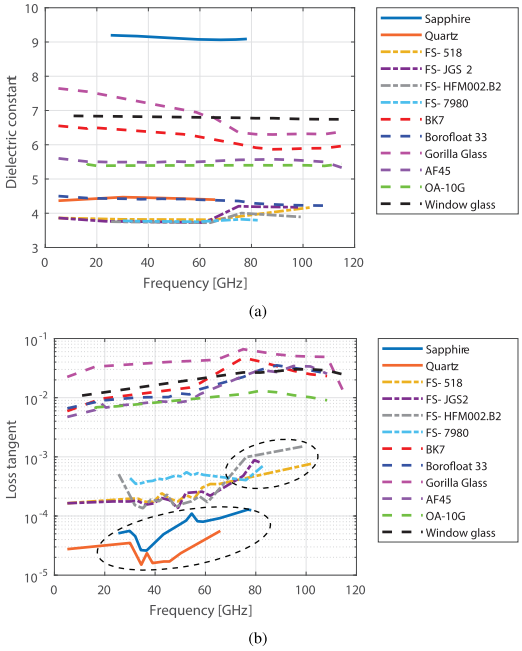

Fig. 4. Characterization of the silicate family until 115 GHz. (a) Dielectric constant (b) Loss tangent. The lower circle represents data points that are near the loss threshold of the open resonator, while the upper circle corresponds of those of the MCK.

any impurities, as Table I shows. The polarizability of fused silica is higher than quartz, as shown in [15], which provides extra movement of the structure, and thus, higher loss. As the percentage of alkali and alkali earth modifiers commences to increase, the dielectric loss increases another order of magnitude. The loss curves have an increasing tendency at around 100 GHz due to the tails of the ionic polarization.

Apart from the minimum measurable loss limitation in resonant techniques, there is also a maximum measurable loss and the value is different for each technique. When the Q factor is relatively low, the resonant peaks are not distinguishable from the noise floor and the 3-dB bandwidth cannot be measured. Therefore, that material is too lossy to be measured. Generally, Q factors below 10 are difficult to measure by resonant methods.

To further elaborate about the properties of glass according to the frequency, the permittivity and dielectric loss evolution of Borofloat 33 are plotted in Fig. 5. The parallel-plate capacitor method has been employed at low frequencies, which requires the metallization of the top and bottom surfaces of the glass. At low frequencies, the higher values of the loss tangent can be attributed to the sodium motion or other impurities on glass. The tails of the dipolar and ionic modes influence microwave and mm-wave loss.

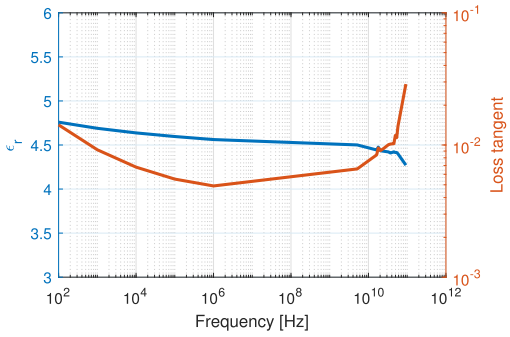

Fig. 5. Dielectric constant and loss tangent of Borofloat 33.

V. Design of a Reflecting Metasurface on Glass

Once the different materials have been characterized, the permittivity and loss tangent values of the substrate at the appropriate frequency can be included in the simulation software. CST studio has been employed as the electromagnetic simulation solver throughout this paper. Periodic boundary conditions are applied in the simulator to obtain the complete response of the full structure.

The design selected for the reflective metasurface is the double-slit split ring resonator (DS-SRR) plotted in Fig. 6 [42], [43]. The chosen operating frequency is 100 GHz and the dimensions are listed in Table IV. The substrate is window glass of 2.3 mm thickness. The metal chosen is aluminum with a thickness of 600 nm.

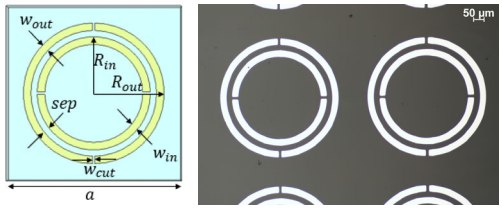

Fig. 6. (a) Unit cell design of the DS-SRR. (b) Microscope image of the fabricated metasurface. The metal appears in white and the glass substrate, in gray. The image was taken with the Nikon L200, which has a magnification up to 100 times.

TABLE IV
DS-SRR DIMENSIONS. UNITS: MM.

R_{out}	0.28	sep	0.028
R_{in}	0.224	a	0.7
w_{out}	0.028	w_{cut}	0.014
w_{in}	0.028		

The metasurface has been manufactured with a lift-off process. This procedure usually starts with a cleanse of the glass with acetone and isopropanol (IPA). However, the adhesion on

the glass was not good enough. Therefore, an oxygen plasma etch was performed at the beginning to remove residues and increase the adhesion. For the lift-off process, two photoresist layers need to be applied. After spin coating the first one, *LOR5A*, a 3-minute bake at $190°C$ is required. The second photoresist is *SPR3012*, with a 1-minute bake at $95°C$. After the soft bake, the sample is ready for the UV exposure in the *MLA 150* with the pattern. When the exposure is done, the sample is developed less than 1 minute in the $CD26$ base. A layer of 600 nm of aluminum is deposited by electron-beam evaporation in the Temescal *FC-2000*. In order to remove the excess resist and metal, the sample is left in a water bath at $87°C$ with *PRS 3000* for a few hours. The resulting metasurface is shown in Fig. 6(b).

The reflecting DS-SRR metasurface has been measured with the SWISSto12 MCK solution, as the frequency of operation is 100 GHz. The measurements are compared, in Fig. 7, with the simulation results of a unit cell illuminated by a plane wave with vertical polarization. Good agreement can be found between measurements and simulation results. At 100 GHz, the reflection coefficient is -1.56 dB in the simulation. There has been a small frequency shift of the resonance frequency to higher frequencies in the measurement. At 101.3 GHz, the reflection coefficient is -1.69 dB. The reflection coefficient is almost 24 dB higher than the transmission coefficient in the measurements.

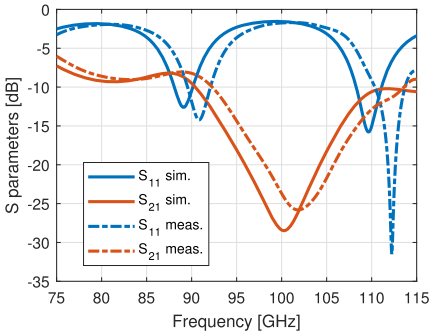

Fig. 7. S parameters comparison between measurements and simulation of the vertical polarization.

In order to provide a better understanding of the performance improvement that the metasurface can achieve; the absorbance, reflectance and transmittance of the DS-SRR is compared with the glass alone in Fig. 8. At the frequency of operation (100 GHz), the reflectance of the DS-SRR is 70%, while the value for the glass alone is 2.5%. Only 0.14% of the signal is transmitted through the DS-SRR, while for the glass, this value is 60%.

1) Dielectric and metal loss study: A dielectric and metal loss study has been conducted around the frequency of operation. In Fig 9(a), the reflection coefficient of the DS-SRR has been plotted for the different silicate materials studied. Quartz has a loss tangent at 100 GHz of around 10^{-4}, fused silica of

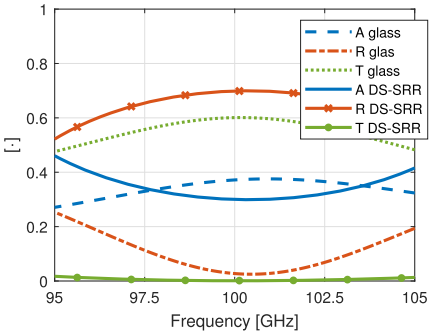

Fig. 8. Absorbance (A), reflectance (R) and transmittance (T) comparison between the DS-SRR metasurface and just window glass.

10^{-3} and glass of 10^{-2}. While there is not too much difference between quartz and fused silica, the reflection coefficient can worsen up to 2.5 dB for glasses. Fig. 9(b) shows the reflection coefficient of the DS-SRR using different kinds of metals. The contrast between the metal conductivity is not as large as for the dielectric loss of the silicate, as the S_{11} only varies around 1 dB. Apart from nickel, the rest of the metals provide a similar response. The plots confirm the theory that the dielectric loss is larger than the metal loss at mm-wave frequencies.

To further extend the analysis, for each loss tangent value (Fig. 10(a)), the minimum value of the reflection coefficient at 100 GHz has been obtained for the different metals and then plotted in a boxplot, and vice versa in Fig. 10(b).

The outlier crosses in Fig. 10(a) are the values corresponding to nickel. They are classified as outliers, as they are greater than $q_3 + 1.5 \times (q_3 - q_1)$, being q_1 and q_3 the 25^{th} and 75^{th} percentiles of the sample data respectively. As was shown in Fig. 9(b), the data is tightly grouped, since the different conductivity of the metals does not make a big difference. It can also be seen that, for a silicate substrate loss higher than 10^{-3}, the minimum reflection coefficient is quite similar (around -0.15 dB). The reflection coefficient worsens to -0.5 dB for glass with $\tan\delta = 10^{-2}$ and to -0.5 dB for $\tan\delta = 2.9 \times 10^{-2}$.

Fig. 10(b) shows similar reflection coefficient values for all the metals, but nickel. The difference between using a substrate with a loss tangent of 2.9×10^{-2} and 10^{-5} is around 2.37 dB.

Finally, to stress the importance of the dielectric characterization in the mm-wave spectrum, we would like to show the simulated difference in performance, if instead of using the permittivity and loss tangent of window glass at 100 GHz, the values of the dielectric at 10 GHz were employed (Fig. 11). There is a 1 dB difference in the reflection coefficient and around 4 dB in the transmission coefficient.

VI. Conclusion

Broadband dielectric characterization of materials is not trivial and requires several techniques as each has a limited

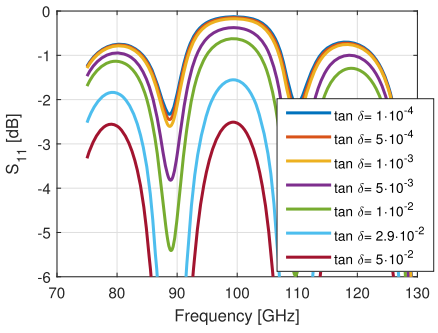

(a)

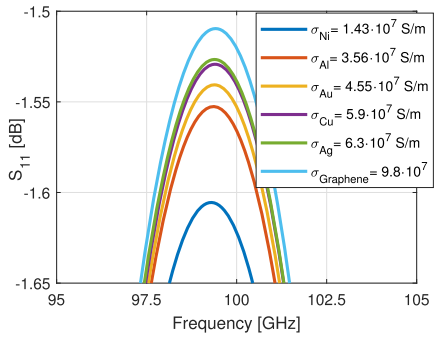

(b)

Fig. 9. Effect of the dielectric and metal loss on the reflection coefficient of the simulated DS-SRR. (a) Loss tangent sweep. (b) Metal conductivity sweep.

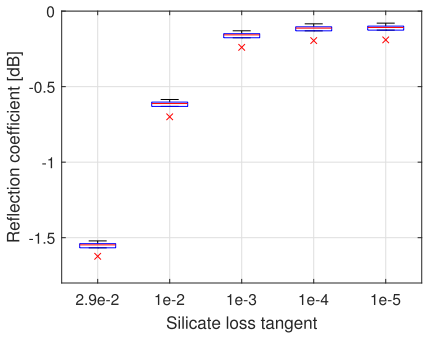

(a)

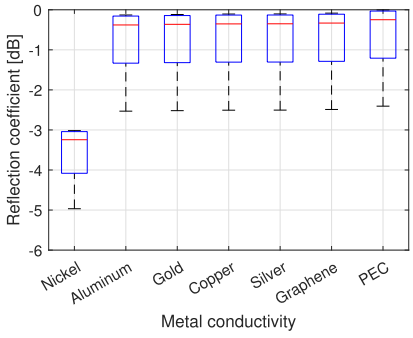

(b)

Fig. 10. Minimum value of the reflection coefficient of the simulated DS-SRR at 100 GHz. (a) Effect of the different metal conductivities for different kinds of silicates. (b) Effect of the silicate loss tangent for different metal conductivities.

operating frequency band or even a single frequency value. Moreover, the loss threshold of each technique is different, with some of them, such as the MCK from SWISSto12, not being able to accurately measure the loss tangent of low loss materials like quartz and fused silica. Besides, each measurement method requires a specific sample size and thickness.

The permittivity values are independent of frequency in the range from 5 to 115 GHz. There is general increase in the loss tangent values with increasing frequency, that can be attributed to the ionic polarization modes.

Both material structure and composition influence the microwave and mm-wave dielectric properties. Amorphous silicates have higher loss values than their crystalline counterparts. Alkaline and alkaline earth additives increase the dielectric permittivity and loss.

The characterization of the materials has allowed having a good simulation model for the split ring resonator metasurfaces on glass and there is good agreement between measurements and simulations. It was demonstrated that the dielectric losses contribute more to device performance than metal losses.

REFERENCES

[1] "5G; NR; Base Station (BS) radio transmission and reception (Release 17)," 3rd Generation Partnership Project (3GPP), Technical Specification (TS) 38.104, 08 2022, version 17.6.0.

[2] Y. Xing and T. S. Rappaport, "Propagation measurement system and approach at 140 ghz-moving to 6g and above 100 ghz," in *2018 IEEE global communications Conference (GLOBECOM)*. IEEE, 2018, pp. 1–6.

[3] Z. Pi and F. Khan, "An introduction to millimeter-wave mobile broadband systems," *IEEE communications magazine*, vol. 49, no. 6, pp. 101–107, 2011.

[4] R. Rodriguez-Cano, "Integration of mm-wave antenna systems in 5G mobile terminals," Ph.D. dissertation, Aalborg Universitet, 2020.

[5] L. Dai, B. Wang, M. Wang, X. Yang, J. Tan, S. Bi, S. Xu, F. Yang, Z. Chen, M. Di Renzo *et al.*, "Reconfigurable intelligent surface-based wireless communications: Antenna design, prototyping, and experimental results," *IEEE Access*, vol. 8, pp. 45 913–45 923, 2020.

[6] M. A. ElMossallamy, H. Zhang, L. Song, K. G. Seddik, Z. Han, and G. Y. Li, "Reconfigurable intelligent surfaces for wireless communications: Principles, challenges, and opportunities," *IEEE Transactions on Cognitive Communications and Networking*, vol. 6, no. 3, pp. 990–1002, 2020.

[7] Y. Liu, X. Liu, X. Mu, T. Hou, J. Xu, M. Di Renzo, and N. Al-Dhahir, "Reconfigurable intelligent surfaces: Principles and opportunities," *IEEE Communications Surveys & Tutorials*, vol. 23, no. 3, pp. 1546–1577, 2021.

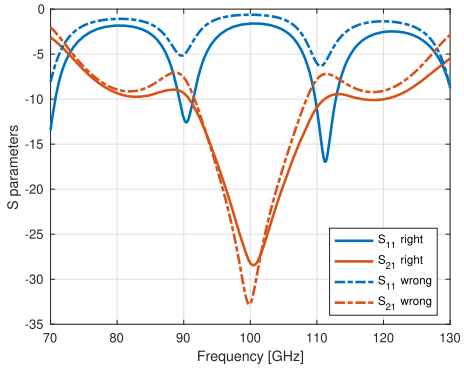

Fig. 11. S parameters simulation comparison of the DS-SRR with the dielectric properties of window glass at 100 GHz (right values: $\epsilon_r = 6.74$ and $\tan\delta = 0.03$) and at 10 GHz (wrong values: $\epsilon_r = 6.84$ and $\tan\delta = 0.01$).

[8] J. Kokkoniemi, V. Hovinen, K. Nevala, and M. Juntti, "Initial results on d band channel measurements in los and nlos office corridor environment," in *2022 16th European Conference on Antennas and Propagation (EuCAP)*. IEEE, 2022, pp. 1–5.

[9] N. Hosseini, M. Khatun, C. Guo, K. Du, O. Ozdemir, D. W. Matolak, I. Guvenc, and H. Mehrpouyan, "Attenuation of several common building materials: millimeter-wave frequency bands 28, 73, and 91 ghz," *IEEE Antennas and Propagation Magazine*, vol. 63, no. 6, pp. 40–50, 2021.

[10] I. Rodriguez, H. C. Nguyen, T. B. Sorensen, J. Elling, J. A. Holm, P. Mogensen, and B. Vejlgaard, "Analysis of 38 ghz mmwave propagation characteristics of urban scenarios," in *Proceedings of European Wireless 2015; 21th European Wireless Conference*. VDE, 2015, pp. 1–8.

[11] B. Salski, J. Cuper, T. Karpisz, P. Kopyt, and J. Krupka, "Complex permittivity of common dielectrics in 20–110 ghz frequency range measured with a fabry–pérot open resonator," *Applied Physics Letters*, vol. 119, no. 5, p. 052902, 2021.

[12] M. Letz, H. Engelmann, G. Lautenschläger, N. Brune, X. Bai, B. Salski, and T. Karpisz, "Special glass for packaging of high frequency electronics," in *2021 51st European Microwave Conference (EuMC)*. IEEE, 2022, pp. 103–106.

[13] K. Hayashi, N. Kidera, and Y. Sato, "Low-loss glass substrates formulated with a variety of dielectric characteristics for millimeter-wave applications," in *2019 IEEE 69th Electronic Components and Technology Conference (ECTC)*. IEEE, 2019, pp. 712–717.

[14] L. Cai, J. Wu, L. Lamberson, E. Streltsova, C. Daly, A. Zakharian, and N. F. Borrelli, "Glass for 5g applications," *Applied Physics Letters*, vol. 119, no. 8, p. 082901, 2021.

[15] M. T. Lanagan, L. Cai, L. A. Lamberson, J. Wu, E. Streltsova, and N. J. Smith, "Dielectric polarizability of alkali and alkaline-earth modified silicate glasses at microwave frequency," *Applied Physics Letters*, vol. 116, no. 22, p. 222902, 2020.

[16] D. D. Chung, "8-ceramic-matrix composites, carbon composites," 2017.

[17] M. T. Lanagan, T. Brown, S. Perini, and Q. X. Yang, "High frequency dielectric materials for medicine and telecommunications," *Japanese Journal of Applied Physics*, vol. 60, no. SF, p. SF0801, 2021.

[18] K. Wakino, M. Murata, and H. Tamura, "Far infrared reflection spectra of ba (zn, ta) o3-bazro3 dielectric resonator material," *Journal of the American Ceramic Society*, vol. 69, no. 1, pp. 34–37, 1986.

[19] H. Tamura, "Microwave dielectric losses caused by lattice defects," *Journal of the European Ceramic Society*, vol. 26, no. 10-11, pp. 1775–1780, 2006.

[20] A. Templeton, X. Wang, S. J. Penn, S. J. Webb, L. F. Cohen, and N. M. Alford, "Microwave dielectric loss of titanium oxide," *Journal of the American Ceramic Society*, vol. 83, no. 1, pp. 95–100, 2000.

[21] G. Brodie, M. V. Jacob, and P. Farrell, "Microwave and radio-frequency technologies in agriculture," in *Microwave and Radio-Frequency Technologies in Agriculture*. De Gruyter Open Poland, 2015, ch. 6.

[22] S. O. Kasap *et al.*, *Principles of electronic materials and devices*. McGraw-Hill New York, 2006, vol. 2.

[23] P. Lunkenheimer, U. Schneider, R. Brand, and A. Loid, "Glassy dynamics," *Contemporary Physics*, vol. 41, no. 1, pp. 15–36, 2000.

[24] A. J. Bur, "Dielectric properties of polymers at microwave frequencies: a review," *Polymer*, vol. 26, no. 7, pp. 963–977, 1985.

[25] F. Kremer and A. Schönhals, *Broadband dielectric spectroscopy*. Springer Science & Business Media, 2002.

[26] R. Geyer, "Dielectric characterization and reference materials," 04 1990.

[27] J. Sheen, "Study of microwave dielectric properties measurements by various resonance techniques," *Measurement*, vol. 37, no. 2, pp. 123–130, 2005.

[28] T. Zwick, A. Chandrasekhar, C. W. Baks, U. R. Pfeiffer, S. Brebels, and B. P. Gaucher, "Determination of the complex permittivity of packaging materials at millimeter-wave frequencies," *IEEE Transactions on Microwave Theory and Techniques*, vol. 54, no. 3, pp. 1001–1010, 2006.

[29] J. Baker-Jarvis, E. J. Vanzura, and W. A. Kissick, "Improved technique for determining complex permittivity with the transmission/reflection method," *IEEE Transactions on microwave theory and techniques*, vol. 38, no. 8, pp. 1096–1103, 1990.

[30] A. L. Cullen and P. Yu, "The accurate measurement of permittivity by means of an open resonator," *Proceedings of the Royal Society of London. A. Mathematical and Physical Sciences*, vol. 325, no. 1563, pp. 493–509, 1971.

[31] T. Grove, M. Masters, and R. Miers, "Determining dielectric constants using a parallel plate capacitor," *American journal of physics*, vol. 73, no. 1, pp. 52–56, 2005.

[32] J. Krupka, A. Gregory, O. Rochard, R. Clarke, B. Riddle, and J. Baker-Jarvis, "Uncertainty of complex permittivity measurements by split-post dielectric resonator technique," *Journal of the European Ceramic Society*, vol. 21, no. 15, pp. 2673–2676, 2001.

[33] M. D. Janezic and J. Baker-Jarvis, "Full-wave analysis of a split-cylinder resonator for nondestructive permittivity measurements," *IEEE Transactions on microwave theory and techniques*, vol. 47, no. 10, pp. 2014–2020, 1999.

[34] G. Kent, "An evanescent-mode tester for ceramic dielectric substrates," *IEEE transactions on microwave theory and techniques*, vol. 36, no. 10, pp. 1451–1454, 1988.

[35] ——, "Nondestructive permittivity measurement of substrates," *IEEE Transactions on Instrumentation and Measurement*, vol. 45, no. 1, pp. 102–106, 1996.

[36] G. Kent and S. M. Bell, "The gap correction for the resonant-mode dielectrometer," *IEEE transactions on instrumentation and measurement*, vol. 45, no. 1, pp. 98–101, 1996.

[37] B. Salski, P. Czekala, T. Karpisz, and P. Kopyt, "Mode coupling in a fabry-perot open resonator," *IEEE Transactions on Microwave Theory and Techniques*, vol. 70, no. 1, pp. 299–306, 2021.

[38] B. Salski, T. Karpisz, M. Warecka, P. Kowalczyk, P. Czekala, and P. Kopyt, "Microwave characterization of dielectric sheets in a plano-concave fabry-perot open resonator," *IEEE Transactions on Microwave Theory and Techniques*, vol. 70, no. 5, pp. 2732–2742, 2022.

[39] Y. Wang, X. Shang, N. M. Ridler, T. Huang, and W. Wu, "Characterization of dielectric materials at wr-15 band (50–75 ghz) using vna-based technique," *IEEE Transactions on Instrumentation and Measurement*, vol. 69, no. 7, pp. 4930–4939, 2019.

[40] Y. Wang, X. Shang, N. M. Ridler, M. Naftaly, A. I. Dimitriadis, T. Huang, and W. Wu, "Material measurements using vna-based material characterization kits subject to thru-reflect-line calibration," *IEEE Transactions on Terahertz Science and Technology*, vol. 10, no. 5, pp. 466–473, 2020.

[41] R. D. Shannon, "Dielectric polarizabilities of ions in oxides and fluorides," *Journal of Applied physics*, vol. 73, no. 1, pp. 348–366, 1993.

[42] R. Marqués, J. Baena, J. Martel, F. Medina, F. Falcone, M. Sorolla, and F. Martín, "Novel small resonant electromagnetic particles for metamaterial and filter design," *Proc. ICEAA*, vol. 3, pp. 439–442, 2003.

[43] J. Bonache, F. Martín, I. Gil, J. García-García, R. Marqués, and M. Sorolla, "Microstrip bandpass filters with wide bandwidth and compact dimensions," *Microwave and Optical Technology Letters*, vol. 46, no. 4, pp. 343–346, 2005.